ChemPubSoc Europe

DOI: 10.1002/celc.201600163

CHEMELECTROCHEM Communications

Special Issue

Investigation of Oxygen Reduction Activity of Catalysts Derived from Co and Co/Zn Methyl-Imidazolate Frameworks in Proton Exchange Membrane Fuel Cells

Lina Chong[+],[a, b] Gabriel A. Goenaga[+],[c] Kia Williams,[d] Heather M. Barkholtz,[a] Lauren R. Grabstanowicz,[e] Jeremy A. Brooksbank,[c] Alex B. Papandrew,[c] Radwan Elzein,[d] Rudiger Schlaf,[d] Thomas A. Zawodzinski, Jr.,[c] Jianxin Zou,[b] Shengqian Ma,[d] and Di-Jia Liu*[a]

We demonstrated that the oxygen reduction reaction (ORR) activity over catalysts derived from pyrolyzed cobalt zeolitic imidazolate frameworks (ZIFs) depends strongly on the imidazole ligand structure and cobalt content. The activity and durability of these catalysts were tested in the proton exchange membrane fuel cell for the first time. The membrane electrode assembly containing a catalyst derived from Co/Zn bimetallic ZIF at the cathode achieved an open-circuit voltage of 0.93 V, a current density of 28 mA cm^{-2} at 0.8 $V_{iR\text{-free}}$, and a peak power density of 374 mW cm^{-2}.

One of the major barriers impeding the large-scale commercialization of proton exchange membrane fuel cells (PEMFCs) lies in the use of high-cost platinum-group metals (PGMs) as electrocatalyst materials, particularly for the oxygen reduction reaction (ORR).[1] Great efforts have been dedicated to the search for nonprecious-metal ORR catalysts as substitutes for PGMs. Extensive studies have been performed on transition-metal (TM)-doped nitrogen and carbon composites ($TM/N_x/C$) as the non-PGM catalysts, with remarkable performance achieved.[2] One of the key challenges for $TM/N_x/C$ ORR catalysts is their relatively low turnover frequency (*TOF*) compared to Pt-based ORR catalysts.[3] To compensate for the low TOF without overusing the catalyst, thus affecting mass transport by excessive electrode layer thickness, the non-PGM catalyst should have as high an active site density as possible. Amorphous carbon as the electrocatalyst support is catalytically inert and dilutes the active site density. An ideal non-PGM catalyst, therefore, should have a high active site density and high specific surface area without the inert carbon support. Another challenge for $TM/N_x/C$, $Fe/N_x/C$ in particular, is that iron could produce hydroxyl and hydroperoxyl radicals through the Fenton reaction from hydrogen peroxide produced during fuel cell polarization.[4] These radicals are highly oxidative and can degrade the polymer membrane and shorten the fuel cell lifespan.[4] Cobalt-based non-PGM catalysts, on the other hand, would have far fewer deleterious effects in this regard.

To address both challenges, we investigated non-PGM catalysts derived from a cobalt-based zeolitic imidazolate framework (ZIF). Specifically, we prepared the catalysts through the pyrolysis of both a monometallic ZIF (cobalt methyl-imidazolate framework $Co(mIm)_2$, or ZIF-67[5]) and a bimetallic ZIF (cobalt/zinc methyl-imidazolate framework $Co/Zn(mIm)_2$, or ZIF-67/8[5]) as a natural extension of our previous investigations of cobalt-based ZIF catalysts.[6] The ORR activities of these catalysts were tested in oxygen-saturated acidic aqueous electrolyte by using the rotating ring-disk electrode (RRDE) method. More importantly, the catalysts were incorporated into the cathode of PEMFCs and evaluated under actual fuel cell operating conditions. Good fuel cell polarization current and power densities were achieved when the fuel cells were operated at 80 °C under 1 bar H_2/O_2 flow. The durability test in the fuel cell showed a decline of cell current density over time for the $Co/Zn(mIm)_2$-derived catalyst. The $Co(mIm)_2$-derived catalyst, on the other hand, demonstrated better stability, albeit at a lower current density. ZIFs, a well-known subfamily of metal-organic frameworks (MOFs), are composed of well-organized metal centers coordinated by bridging imidazolate linkers.[5] In our initial work, we reported the first non-PGM catalyst derived from cobalt H-imidazolate frameworks [Co-ZIF or $Co(Im)_2$]. The catalyst demonstrated promising ORR activity, benefiting from the large number of active centers evenly and regularly prearranged in the porous ZIF precursor structure.[6] The versatility

[a] *L. Chong,[+] H. M. Barkholtz, Dr. D.-J. Liu*
Chemical Sciences and Engineering Division
Argonne National Laboratory
Argonne, IL, 60439 (USA)
E-mail: djliu@anl.gov

[b] *L. Chong,[+] Prof. Dr. J. Zou*
Engineering Research Center of Light Alloy Net Forming and
State Key Laboratory of Metal Matrix Composites
Shanghai Jiao Tong University, Shanghai (P.R. China)

[c] *Dr. G. A. Goenaga,[+] J. A. Brooksbank, Dr. A. B. Papandrew,*
Prof. Dr. T. A. Zawodzinski, Jr.
Chemical and Biomolecular Engineering Department
University of Tennessee, Knoxville, TN 37996 (USA)

[d] *K. Williams, R. Elzein, Prof. Dr. R. Schlaf, Prof. Dr. S. Ma*
University of South Florida
Tampa, FL 33620 (USA)

[e] *Dr. L. R. Grabstanowicz*
Alcoa Technical Center
New Kensington, PA 15068 (USA)

[+] *These authors contributed equally to this work and should be regarded as co-first authors*

Supporting Information for this article can be found under http://dx.doi.org/10.1002/celc.201600163.

Special Issue Invited contribution to a Special Issue on Electrocatalytic Nanomaterials

of MOF/ZIF structures also provides enormous opportunities for further enhancement of the catalyst's ORR performance through rational design, which led to a number of studies in recent years.[2h,i,6,7] During our investigation of ZIF-based non-PGM catalysts, we observed a number of important factors that impact the final catalyst performance. For example, by introducing an alkyl group in 2-position of the imidazole in ZIF, the final catalyst tends to maintain a higher surface area and porosity with more uniform morphology, which are important for optimal ORR catalyst performance. Controlling the TM (Fe or Co) loading also plays an important role in the catalyst performance. Studies have suggested that the metal loading should be kept below 5 wt% in the final catalyst after pyrolysis.[2i] A Fe- or Co-based monometallic ZIF typically contains more than 30 or 40 wt% metal after high-temperature pyrolysis, which is too high to achieve optimal catalytic activity. In this study, we first prepared a Co-based ZIF-derived catalyst by replacing the imidazole ligand in $Co(Im)_2$ with 2-methyl-1*H*-imidazole to form $Co(mIm)_2$ (ZIF-67),[8] followed, first, by thermal activation through an acid wash and, second, by heat treatment under NH_3. The ORR performances of both catalysts were tested in O_2-saturated 0.1 M $HClO_4$ solution by using the RRDE method, and the catalyst derived from $Co(mIm)_2$ outperformed that from $Co(Im)_2$. The new catalyst has sufficient catalytic activity and a suitable surface morphology to be fabricated into the cathode of a membrane electrode assembly (MEA) and tested under PEMFC operating conditions. To control the Co loading in the catalyst, a bimetallic cobalt and zinc ZIF, $Co/Zn(mIm)_2$, was also synthesized and converted to a catalyst. Unlike Co, the Zn in the ZIF will be vaporized at pyrolysis temperatures above 907 °C;[2e,i] therefore, the cobalt loading in the final catalyst can simply be adjusted by controlling the cobalt-to-zinc ratio in the ZIF precursor. The catalyst derived from the bimetallic ZIF showed further catalytic activity improvement in both RRDE and PEMFC tests. An areal current density of 28 mA cm^{-2} at 0.8 $V_{iR\text{-free}}$ and a peak power density of 374 mW cm^{-2} were achieved for the MEA/fuel cell study under 0.5 bar oxygen backpressure.

The synthesis of both $Co(mIm)_2$ and $Co/Zn(mIm)_2$ for pyrolysis were carried out in solution through the reaction between 2-methyl-1*H*-imidazole with $Co(NO_3)_2{\cdot}6H_2O$ and/or $Zn(NO_3)_2{\cdot}6H_2O$ in methanol or water at room temperature, as was previously reported.[5,9] The reactions to form both ZIFs, as well as that of $Co(Im)_2$, are given in reaction schemes in the Supporting Information [Equations (S1)–(S3)]. A representative lattice structure of $Co(mIm)_2$ is shown in Figure S1. The powder X-ray diffraction (XRD) patterns (Figure S2) were identical for $Co(mIm)_2$ and $Co/Zn(mIm)_2$, indicating identical lattice structures.[5] The ORR catalysts were obtained through the pyrolysis of the ZIF crystals. For the $Co(mIm)_2$-derived catalyst, the ZIF precursor was pyrolyzed at 750 °C for 1 h under Ar. An acid-washing step was subsequently applied to remove the leached metals, followed by a second heat treatment at 750 °C for 0.5 h under NH_3. The prepared catalyst is thus named $Co(mIm)_2$-P. For comparison, a similar process was used to prepare the $Co(Im)_2$-derived catalyst, named $Co(Im)_2$-P. For the $Co/Zn(mIm)_2$-derived catalyst, the bimetallic ZIF with a mole ratio of Co/Zn = 5:95 was pyrolyzed at 1000 °C under Ar for 1 h. After an acidic wash, the pyrolyzed sample was treated at 950 °C under NH_3 for 0.5 h to obtain the catalyst $Co/Zn(mIm)_2$-P. The catalytic activities were studied by using the RRDE method. Figure 1 shows the current–potential polarization

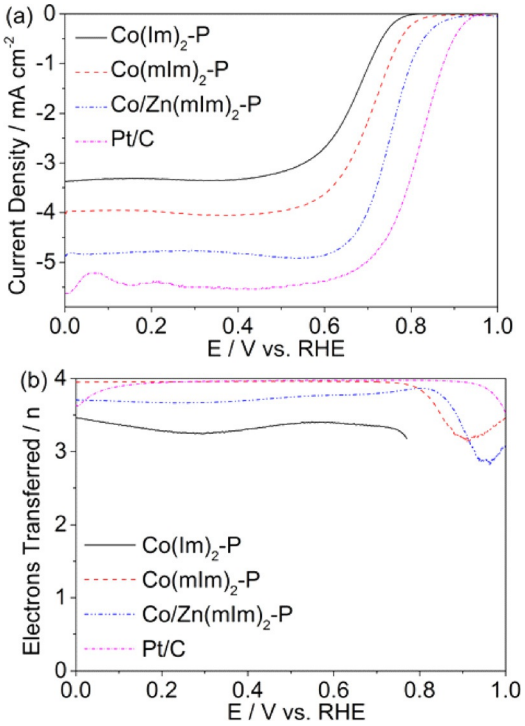

Figure 1. a) Polarization curves of $Co(Im)_2$-P, $Co(mIm)_2$-P, $Co/Zn(mIm)_2$-P, and commercial Pt/C measured by using RRDE in O_2-saturated 0.1 M $HClO_4$ solution at 25 °C, rotation speed = 1600 rpm; b) number of electrons transferred for all four catalysts as a function of the polarization potential.

curves obtained from linear sweep voltammetry (LSV) with the rotating disk at 1600 rpm. $Co(mIm)_2$-P demonstrated good ORR catalytic activity compared to that of $Co(Im)_2$-P with the onset potential, E_0, shifted from 0.81 V for $Co(Im)_2$-P to 0.86 V for $Co(mIm)_2$-P. Meanwhile, the limiting current density measured at 0.2 V increased from 3.4 mA cm^{-2} for $Co(Im)_2$-P to 4 mA cm^{-2} for $Co(mIm)_2$)-P. The half-wave potential, $E_{1/2}$, represents an important gauge of the electrocatalytic activity in the kinetic region. As illustrated in Figure 1, $E_{1/2}$ of $Co(mIm)_2$-P is nearly 40 mV higher than that of $Co(Im)_2$-P. Correspondingly, an improvement in mass activity of $Co(mIm)_2$-P over $Co(Im)_2$-P was also obtained (Figure S3 a). As aforementioned, we expect that $Co/Zn(mIm)_2$-P, with a substantially lower cobalt content in the final catalyst composition, should have significantly improved performance. Indeed, the catalyst exhibited further improved E_0 and $E_{1/2}$ values of 0.93 and 0.76 V, respectively, together with the improved mass activity (Figure S3 a). For comparison, LSV of a commercial Pt/C catalyst (TKK, 47.6 wt% Pt) is also provided in Figure 1, which has an $E_{1/2}$ value of 0.82 V and is only 60 mV higher than that of $Co/Zn(mIm)_2$-P. The electron-transfer number, *n*, at different polarization potentials represents the degree of conversion from oxygen to water in ORR, with *n*

close to 4, indicating almost complete oxygen reduction. This value can be obtained from the ratio of the disk current over the ring current [Eq. (S4)]. The *n* values of all three catalysts are plotted in Figure 1b and are all close to 4. Interestingly, $Co(mIm)_2$-P exhibits the best *n* value number, nearly the same as Pt/C, although not the best E_0 and $E_{1/2}$ of the three. This behavior was confirmed through repeated measurements. The observation suggests that $Co(mIm)_2$-P provided the most complete reduction of molecular oxygen to water, possibly owing to a closer proximity among the active sites, as the distance between two adjacent Co/N/C sites is anticipated to be shorter than that in $Co/Zn(mIm)_2$-P, because of the difference in Co concentration in the precursors. Such proximity could result in more effective sequential electron transfer to the peroxide intermediates formed on the catalyst surface, leading to more complete oxygen reduction. Verifying the true mechanism requires a more detailed mechanistic study. The lower limiting current density of $Co(mIm)_2$-P compared to $Co/Zn(mIm)_2$-P is attributed to incomplete ink coverage on the RRDE electrode surface. Such a phenomenon is often observed in non-PGM catalysts with high metal loading, where particles of encapsulated metal crystallites, carbide, and nitride are often observed. Table 1 summarizes the key catalytic performance parameters derived from RRDE measurements for all three catalysts.

Table 1. Electrocatalytic performance and surface properties of catalysts measured by using RRDE and BET methods.

Catalyst	E_0 [V][a]	$E_{1/2}$ [V]	*n* value	BET SSA[b] [$m^2 g^{-1}$]	Micropore diameter [Å]
$Co(Im)_2$-P	0.81	0.67	3.3–3.6	434[6]	10–12
$Co(mIm)_2$-P	0.86	0.71	3.9–3.95	621	4–8
$Zn/Co(mIm)_2$-P	0.93	0.76	3.7–3.8	1563	6–9, 11–16
Pt/C	0.95	0.82	3.6–3.95	–	

[a] V vs. RHE, read at 0.003 mA cm^{-2} from Figure 1a. [b] BET surface area and pore-size distribution data were measured by using nitrogen sorption isotherms at 77 K within a domain of P/P_0 from 0–1; pore-size distribution was calculated by using the cylinder model with the NLDFT method.

In a ZIF-derived catalyst, the active sites are uniformly distributed throughout the surface and there is no distinction between the catalyst and support regions.[2b,h] Maximizing the specific surface area (SSA) is therefore equivalent to maximizing the catalytic active area. We measured the catalysts' Brunauer–Emmett–Teller (BET) SSAs by using the N_2 adsorption isotherm at 77 K, and obtained SSAs of 621 $m^2 g^{-1}$ for $Co(mIm)_2$-P (Figure S4) and 434 $m^2 g^{-1}$ for $Co(Im)_2$-P[6]. $Co/Zn(mIm)_2$-P has the highest surface area among all of the samples (1563 $m^2 g^{-1}$), with the micropore size distribution being around 6–9 Å and 11–16 Å (Figure S5), occupying 86% of total area in pore. Besides the surface property, the N content in the pyrolyzed catalyst has been considered as another important factor contributing to the catalytic ORR activity.[2b] The elemental analyses of Co, C, and N in $Co(mIm)_2$-P and $Co/Zn(mIm)_2$-P were performed by using energy-dispersive X-ray spectroscopy (EDS) and the results are listed in Table S1. The analyses indicate a slight increase in the nitrogen content in $Co/Zn(mIm)_2$-P with respect to $Co(mIm)_2$-P, but the latter has a substantially higher cobalt content, even after the acid wash. N 1s spectra were further studied by using X-ray photoelectron spectroscopy (XPS) for $Co(Im)_2$-P, $Co(mIm)_2$-P, and $Co/Zn(mIm)_2$-P, which were found to be primarily composed of pyridinic and pyrrolic N, with the former being the more dominant component (Figure S6 and Table S2). The similar observation was also reported in our previous investigation on $Co(Im)_2$-P.[6] A higher nitrogen content could lead to the formation of additional catalytic centers[2i] and this, combined with the higher surface area (1563 $m^2 g^{-1}$), account for the superior catalytic activity of the $Co/Zn(mIm)_2$-P sample.[2e,h,i] The XRD pattern shows that Co^0 appears in the $Co(mIm)_2$-P sample (Figure S2). Figure 2a shows

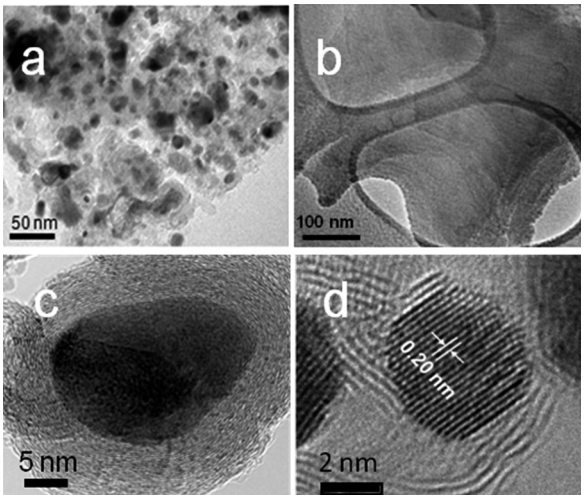

Figure 2. TEM images of a) $Co(mIm)_2$-P and b) bimetallic $Co/Zn(mIm)_2$-P. c, d) HRTEM images of Co nanoparticles in $Co(mIm)_2$-P.

the transmission electron microscopy (TEM) image of $Co(mIm)_2$-P. Dark, but inhomogeneous, particles with a diameter around 10–20 nm embedded in the carbon matrix were detected, similar to what we observed in our previous study for $Co(Im)_2$-P.[6] High-resolution (HR)TEM further confirmed the existence of metallic Co with a typical lattice spacing of 0.20 nm (Figures 2c and 2d), which is consistent with the XRD results (Figure S2). These particles were encapsulated inside of graphitic layers and, therefore, cannot be removed, even after thorough acid washing.[6] For $Co/Zn(mIm)_2$-P, the morphology is somewhat different. Figure 2b shows a highly porous carbon structure without visible metal nanoparticles. Such a structure is similar to our previous study on pyrolyzed tris-1,10-phenanthroline iron (II) perchlorate (TPI) mixed with ZIF-8.[7] Nonetheless, Co nanoparticles were detected by using XRD, albeit at a much weaker intensity, implying some sparsely dispersed Co particles still exist in $Co/Zn(mIm)_2$-P after heating at 1000 °C.

The improved catalytic activity of $Co/Zn(mIm)_2$-P was further demonstrated through a MEA/fuel cell test. For comparison, a fuel cell test on the $Co(mIm)_2$-P sample was also performed under the same test conditions. Figure 3a shows the cell voltages and power densities as functions of the current density,

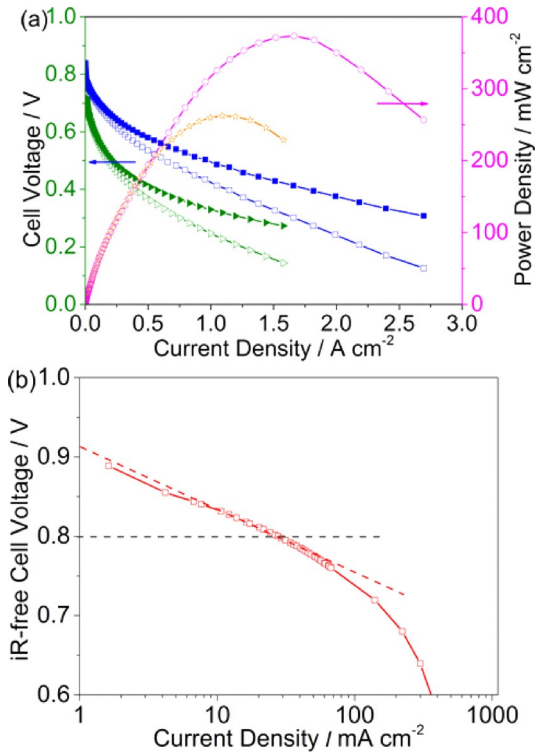

Figure 3. a) Cell voltages and power densities as a function of the current density measured in single cell tests with $Co(mIm)_2$-P and $Co/Zn(mIm)_2$-P as the cathode catalysts, respectively. For the cathode, the catalyst loading was 1.6 mg cm^{-2} with an ionomer-to-catalyst ratio (*I*/*C*) of 0.86:1; for the anode, the catalyst loading was 0.4 mg_{Pt} cm^{-2} prepared with 20 wt% Pt/C. Nafion 211 was used as the membrane. The absolute pressures of O_2 and H_2 were kept at 1 bar under 100% RH (back pressure = 0.5 bar). The temperature was maintained at 80 °C. ■: $Co/Zn(mIm)_2$-P (IR-free); □: $Co/Zn(mIm)_2$-P (uncorrected); ▶: $Co(mIm)_2$-P (IR-free): ▽: $Co(mIm)_2$-P (uncorrected). ○: $Co/Zn(mIm)_2$-P-power density; *:$Co(mIm)_2$-P- power density. b) Tafel plot of another MEA/single cell with $Co/Zn(mIm)_2$-P as the cathode catalyst with loading = 4 mg cm^{-2}. The rest of cell test conditions are identical to (a).

using either $Co/Zn(mIm)_2$-P or $Co(mIm)_2$-P as the cathode catalyst. The cathode catalyst loadings were 1.6 mg cm^{-2} for both samples and Nafion 211 membrane was used in both MEAs. Figure 3a demonstrates the dramatically improved fuel cell performance of $Co/Zn(mIm)_2$-P compared with that of $Co(mIm)_2$-P in terms of open-circuit voltage (OCV) and the cell voltage in the entire span of the polarization current density. Furthermore, the peak power density also increased from 250 mW cm^{-2} for $Co(mIm)_2$-P to 374 mW cm^{-2} for the $Co/Zn(mIm)_2$-P sample. To better evaluate the fuel cell performance in the kinetic region, another MEA with $Co/Zn(mIm)_2$-P at the cathode was also prepared and tested under similar conditions. Figure 3b shows the Tafel plot derived from the *iR*-corrected polarization curve. An areal current density of 28 mA cm^{-2} was achieved at 0.8 $V_{iR\text{-free}}$ and the OCV reached 0.91 V.

The stabilities of $Co/Zn(mIm)_2$-P and $Co(mIm)_2$-P were also investigated in the single fuel cell tests. The tests were carried out at a constant voltage of 0.5 V with air as the cathode feed. Figure 4 shows the change of fuel cell current densities as a function of the running time of the fuel cells. For the fuel

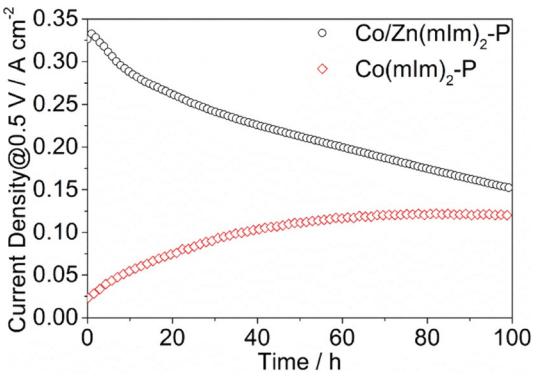

Figure 4. Current density as a function of time tested under a constant voltage of 0.5 V in the fuel cells with $Co(mIm)_2$-P and bimetallic $Co/Zn(mIm)_2$-P as the cathode catalysts. The catalyst loadings were 1.6 mg cm^{-2} with Nafion 211 as the membrane. Test conditions: air = H_2 = 1 bar (back pressure = 0.5 bar), temperature = 80 °C, RH = 100%.

cell with $Co/Zn(mIm)_2$-P as the cathode catalyst, the current density decreased to 0.152 A cm^{-2} from an initial value of 0.336 A cm^{-2}, representing a 45% loss during the 100 h aging test. Such loss of activity is similar in the previously reported fuel cell tests using a catalyst derived from iron-decorated ZIF-8.[2e,i] For the fuel cell with $Co(mIm)_2$-P as the cathode catalyst, the cell current actually increased gradually during the first 50 h, before reaching a constant level of 0.125 A cm^{-2}. We attribute such gradual increase to the "break-in" period needed for a highly graphitized catalyst material such as $Co(mIm)_2$-P. In a separate fuel cell, we further studied the $Co(mIm)_2$-P durability by collecting the polarization curves every 50 h in fully humidified H_2/O_2 for up to 350 h (Figure S7). The catalyst showed reasonably good stability from the 50th hour to the 350th hour. As was demonstrated before, a higher level of graphitization usually leads to a more stable ORR catalyst,[10] which is presumably because of the better preservation of active sites under oxidative conditions at the cathode. We performed Raman spectroscopic measurements for all three samples and found that $Co(mIm)_2$-P and $Co(Im)_2$-P have similar levels of graphitization, whereas $Co/Zn(mIm)_2$-P was the least graphitized among the three (Figure S8 and Table S3). The current study demonstrates the need to balance the catalyst's SSA and graphitization, which are often difficult to optimize simultaneously. On one hand, $Co/Zn(mIm)_2$-P provides a very high surface area and less graphitization, presumably owing to the release of Zn at elevated temperature, which interrupts the graphitic lattice formation. The high SSA offers a higher number of active sites and, therefore, better initial activity. These active sites over the amorphous support, however, are less stable under the corrosive environment in the cathode. On the other hand, $Co(mIm)_2$-P has a lower surface area but is more graphitic in nature, which may be attributed to graphitization catalyzed by the presence of a high amount of cobalt.[2f] The graphitic carbon has a stronger resistance to oxidative corrosion and, thus, better stability. This stability gain, however, is at the expense of a reduction in catalytic activity. At present, cobalt ZIF-based nonprecious catalysts are outperforming some early Co-based systems.[11] As research on nonprecious-metal catalysts

progresses, it is important to strike a balance between the different surface/morphology properties in searching for more active and durable materials.

In summary, we demonstrated the importance of imidazole ligand structure and cobalt concentration in terms of the ORR activity and durability in nonprecious-metal catalysts derived from pyrolyzed cobalt-based ZIFs. For the first time, these Co–ZIF-based catalysts are fabricated into the cathode of the MEAs and tested under PEMFC operating conditions. We found that alkyl substitution in the imidazole ligand led to the improvement of the catalyst activity. Controlling the cobalt loading by replacing Co^{+2} with Zn^{+2} in the zeolitic methylimidazolate frameworks increased the pyrolyzed catalytic activity substantially. The catalytic performance study, combined with the surface property investigation, suggests that there is a trade-off between the catalyst activity and durability, which could be a balance between the SSA and the graphitization level. The future prospects of such nonprecious-metal catalysts depends on successful advances in both fronts of the catalyst properties.

Experimental Section

Details of the Co-based ZIF precursor syntheses, ORR catalyst preparations, MEA fabrication, RRDE and single cell tests, as well as catalyst stability investigations are provided in the Supporting Information.

Acknowledgements

The authors wish to thank Dr. Magali Ferrandon for her support in XRD characterization. D.-J.L. wishes to thank US. Department of Energy, Office of Energy Efficiency and Renewal Energy, Fuel Cell Technologies Office and Office of Sciences for their financial support of this work. L.C. wishes to acknowledge Chinese Scholarship Council for its financial support. J.Z. would like to thank support from the Science and Technology Commission of Shanghai Municipality under grant No. 14JC1491600. Argonne National Laboratory is a U.S. Department of Energy, Office of Science Laboratory operated under Contract No. DEAC02-06CH11357 by UChicago Argonne, LLC.

Keywords: electrocatalysts · cobalt · fuel cells · metal-organic frameworks · oxygen reduction reaction

[1] H. A. Gasteiger, S. S. Kocha, B. Sompalli, F. T. Wagner, *Appl. Catal. B* **2005**, *56*, 9–35.

[2] a) C. W. B. Bezerra, L. Zhang, K. Lee, H. Liu, A. L. B. Marques, E. P. Marques, H. Wang, J. Zhang, *Electrochim. Acta* **2008**, *53*, 4937–4951; b) F. Jaouen, J. Herranz, M. Lefevre, J.-P. Dodelet, U. I. Kramm, I. Herrmann, P. Bogdanoff, J. Maruyama, T. Nagaoka, A. Garsuch, J. R. Dahn, T. Olson, S. Pylypenko, P. Atanassov, E. A. Ustinov, *ACS Appl. Mater. Interfaces* **2009**, *1*, 1623–1639; c) M. Lefevre, E. Proietti, F. Jaouen, J.-P. Dodelet, *Science* **2009**, *324*, 71–74; d) F. Jaouen, E. Proietti, M. Lefevre, R. Chenitz, J.-P. Dodelet, G. Wu, H. T. Chung, C. M. Johnston, P. Zelenay, *Energy Environ. Sci.* **2011**, *4*, 114–130; e) E. Proietti, F. Jaouen, M. Lefèvre, N. Larouche, J. Tian, J. Herranz, J.-P. Dodelet, *Nat. Commun.* **2011**, *2*, 416; f) G. Wu, K. L. More, C. M. Johnston, P. Zelenay, *Science* **2011**, *332*, 443–447; g) R. Bashyam, P. Zelenay, *Nature* **2006**, *443*, 63–66; h) D. Zhao, J.-L. Shui, L. R. Grabstanowicz, C. Chen, S. M. Commet, T. Xu, J. Lu, D.-J. Liu, *Adv. Mater.* **2014**, *26*, 1093–1097; i) D. Zhao, J.-L. Shui, C. Chen, X. Chen, B. M. Reprogle, D. Wang, D.-J. Liu, *Chem. Sci.* **2012**, *3*, 3200–3205; j) S. Yuan, J.-L. Shui, L. Grabstanowicz, C. Chen, S. Commet, B. Reprogle, T. Xu, L. Yu, D.-J. Liu, *Angew. Chem. Int. Ed.* **2013**, *52*, 8349–8353; *Angew. Chem.* **2013**, *125*, 8507–8511.

[3] A. A. Gewirth, M. S. Thorum, *Inorg. Chem.* **2010**, *49*, 3557–3566.

[4] I. C. Halalay, B. A. Merzougui, A. M. Mance, *ECS Trans.* **2008**, *16*, 969–981.

[5] R. Banerjee, A. Phan, B. Wang, C. Knobler, H. Furukawa, M. O'Keeffe, O. M. Yaghi, *Science* **2008**, *319*, 939–943.

[6] S. Ma, G. A. Goenaga, A. V. Call, D.-J. Liu, *Chem. Eur. J.* **2011**, *17*, 2063–2067.

[7] J. Shui, C. Chen, L. Grabstanowicz, D. Zhao, D. J. Liu, *Proc. Natl. Acad. Sci. USA* **2015**, *112*, 10629–10634.

[8] G. Goenaga, S. Ma, S. Yuan, D.-J. Liu, *ECS Trans.* **2010**, *33*, 579–586.

[9] a) A. V. Kuttatheyil, D. Laessig, J. Lincke, M. Kobalz, M. Baias, K. Koenig, J. Hofmann, H. Krautscheid, C. J. Pickard, J. Haase, M. Bertmer, *Inorg. Chem.* **2013**, *52*, 4431–4442; b) X. Wang, J. Zhou, H. Fu, W. Li, X. Fan, G. Xin, J. Zheng, X. Li, *J. Mater. Chem. A* **2014**, *2*, 14064; c) X. Fan, W. Wang, W. Li, J. Zhou, B. Wang, J. Zheng, X. Li, *ACS Appl. Mater. Interfaces* **2014**, *6*, 14994–14999; d) B. You, N. Jiang, M. Sheng, W. S. Drisdell, J. Yano, Y. Sun, *ACS Catal.* **2015**, *5*, 7068–7076.

[10] H. Meng, N. Larouche, M. Lefevre, F. Jaouen, B. Stansfield, J.-P. Dodelet, *Electrochim. Acta* **2010**, *55*, 6450–6461.

[11] a) T. S. Olson, K. Chapman, P. Atanassov, *J. Power Sources* **2008**, *183*, 557–563; b) H.-C. Huang, I. Shown, S.-T. Chang, H.-C. Hsu, H.-Y. Du, M.-C. Kuo, K.-T. Wong, S.-F. Wang, C.-H. Wang, L.-C. Chen, K.-H. Chen, *Adv. Funct. Mater.* **2012**, *22*, 3500–3508.

Manuscript received: March 30, 2016
Accepted Article published: May 19, 2016
Final Article published: May 31, 2016